Recovery of ordered periodic orbits with increasing wavelength for sound propagation in a range-dependent waveguide

L. E. Kon'kov, D. V. Makarov,* E. V. Sosedko, and M. Yu. Uleysky
V. I. Il'ichev Pacific Oceanological Institute of the Russian Academy of Sciences, 690041 Vladivostok, Russia
(Received 25 July 2007; revised manuscript received 16 October 2007; published 16 November 2007)

We consider sound wave propagation in a range-periodic acoustic waveguide in the deep ocean. It is demonstrated that vertical oscillations of a sound-speed perturbation, induced by ocean internal waves, influence near-axial rays in a resonant way, producing ray chaos and forming a wide chaotic sea in the underlying phase space. We study interplay between chaotic ray dynamics and wave motion with signal frequencies of 50–100 Hz. The Floquet modes of the waveguide are calculated and visualized by means of the Husimi plots. Despite of irregular phase space distribution of periodic orbits, the Husimi plots display the presence of ordered peaks within the chaotic sea. These peaks, not being supported by certain periodic orbits, draw the specific "chainlike" pattern, reminiscent of KAM resonance. The link between the peaks and KAM resonance is confirmed by ray calculations with lower amplitude of the sound-speed perturbation, when the periodic orbits are well-ordered. We associate occurrence of the peaks with the recovery of ordered periodic orbits, corresponding to KAM resonance, due to suppressing of wave-field sensitivity to small-scale features of the sound-speed profile that take place with increasing wavelength.

DOI: 10.1103/PhysRevE.76.056212 PACS number(s): 05.45.Ac, 05.45.Mt, 43.30.+m, 92.10.Vz

I. INTRODUCTION

In recent years interrelation between wave-field structure and its semiclassical description has attracted increasing attention in the context of wave chaos—wave-field manifestations of ray chaos. Ray chaos means instability of ray trajectories, conditioned by nonintegrability of the classical Hamiltonian equations and is found to be the essential part of wave propagation in various environments, ranging from artificial optical devices [1] to natural media [2–4]. In addition, the problem of wave chaos is closely connected to the problem of quantum chaos, which is understood as quantum dynamics of classically chaotic systems [5].

The present paper is devoted to long-range sound propagation in the ocean, which has become of growing interest in recent decades [6–9]. Increasing of pressure with depth, combined with the warming of the upper oceanic layer, results in nonmonotonic dependence of the sound speed on depth. According to Snell's law, there occurs a waveguide confining acoustic waves within a restricted water volume and preventing their interaction with the lossy bottom. When we deal with guided wave propagation, weak inhomogeneities along the axis of propagation may be sufficient for dividing phase space into regular and irregular regions [10]. This division, relying on the Kolmogorov-Arnold-Moser (KAM) theory, even persists in the case of a stochastically perturbed waveguide [11,12], giving rise to coherent ray clusters [13]. Ray chaoticity leads to smearing of a spatial wave-field structure due to irregular mode coupling [14,15], randomlike distribution of ray arrival times at the receiver [16,17], or anomalous transmission loss due to the chaos-assisted ray escaping from a waveguide [18,19].

On another front, it is well established that a wave packet may demonstrate coherent or incoherent motion depending upon whether the initial position of a wave packet is in the regular or irregular part of classical phase space [20,21]. The packet initially concentrated inside a region of stability remains localized, while the packet placed within a chaotic region spreads rapidly. In contrast to the semiclassical limit, boundaries between stable and chaotic regions are penetrable at nonzero wavelength. This enables extension of a wave packet, evolving in the chaotic region, into an area with regular dynamics; the effect is amplifying with increasing wavelength [22]. Thus wave corrections imply suppressing of the phase space separation.

Chaos means irregular behavior of rays and can be thought of as purely refractional phenomena. The description of chaos-induced effects in wave motion far from the semiclassical limit requires the understanding of how wave refraction depends on wavelength. This issue is of great importance in the presence of small-scale features, which seem to be irrelevant for wave refraction at low frequencies [23]. In underwater acoustics, these features are usually associated with internal waves. In the present paper we follow two aims. First, we study the effect of small-scale vertical oscillations of a perturbation on ray dynamics. We shall show that these oscillations account for strong chaos of near-axial rays. Second, we investigate interrelation between strong chaos of near-axial rays and the wave-field structure at low frequencies.

The paper is organized as follows. In the next section we describe briefly the model of a waveguide. Section III is devoted to classical ray dynamics. In Sec. IV we study wave-field properties by means of Husimi representation of the Floquet modes. In the Conclusion, we shortly discuss the results obtained.

II. MODEL OF A WAVEGUIDE

Consider a monochromatic wave field in a two-dimensional acoustic waveguide in the deep ocean with the sound speed c presented in the form

*makarov@poi.dvo.ru

$$c(z,r) = c_0 + \Delta c(z) + \delta c(z,r), \tag{1}$$

where c_0 is a reference sound speed, $\Delta c(z)$ represents the range-independent depth change of the sound speed due to the waveguide, and $\delta c(z,r)$ is a small term varying with range r. In the present paper we give consideration to the narrow-angle wave propagation, when the original Helmholtz equation for a wave field reduces to the parabolic equation

$$\frac{i}{k_0}\frac{\partial \phi(z,r)}{\partial r} = \hat{H}\phi(z,r),$$

$$\hat{H} = -\frac{1}{2k_0^2}\frac{\partial^2}{\partial z^2} + \frac{\Delta c(z) + \delta c(z,r)}{c_0}. \tag{2}$$

Here $k_0 = 2\pi f/c_0$ is the wave number in the reference medium with $c = c_0$ and f is the signal frequency. The parabolic equation formally coincides with the nonstationary Schrödinger equation. In this analogy one treats range r as the timelike variable, $\Delta c(z)$ as an unperturbed potential, δc as a time-dependent perturbation, and k_0^{-1} as the Planck constant.

In the present paper we shall consider an idealistic model of a waveguide with $\Delta c(z)$ and $\delta c(z,r)$ given by the following expressions:

$$\Delta c(z) = -\frac{c_0 b^2}{2}(\mu - e^{-az})(e^{-az} - \gamma), \tag{3}$$

$$\delta c(z,r) = \varepsilon c_0 \frac{z}{B} e^{-2z/B} \sin\frac{2\pi z}{\lambda_z}\sin\frac{2\pi r}{\lambda_r}, \tag{4}$$

where $c_0 = c(z=h) = 1535$ m/s, $\gamma = \exp(-ah)$, $h = 4.0$ km is depth of the ocean bottom, $\mu = 1.078$, $a = 0.5$ km^{-1}, $b = 0.557$, $\varepsilon = 0.005$, $B = 1$ km, $\lambda_z = 0.2$ km, and $\lambda_r = 5$ km. Function $\Delta c(z)$ takes on the smallest value at the depth

$$z_a = \frac{1}{a}\ln\frac{2}{\mu + \gamma} \simeq 1 \text{ km}. \tag{5}$$

We shall refer to this depth as the channel axis. The respective unperturbed sound-speed profile is depicted in Fig. 1(a). Fast oscillations of $\delta c(z,r)$ are included in order to mimic the effect of internal wave fine structure and distort the sound-speed profile, as is demonstrated in Fig. 1(b).

III. RAY DYNAMICS

The classical counterpart of the operator $\hat{H}$ is the Hamiltonian

$$H = -1 + \frac{p^2}{2} + \frac{\Delta c(z)}{c_0} + \frac{\delta c(z,r)}{c_0}, \tag{6}$$

where $p = \tan\alpha$ is the analog to mechanical momentum and α is a grazing angle of a sound ray. Ray trajectories obey the Hamiltonian equations

$$\frac{dz}{dr} = \frac{\partial H}{\partial p} = p, \tag{7}$$

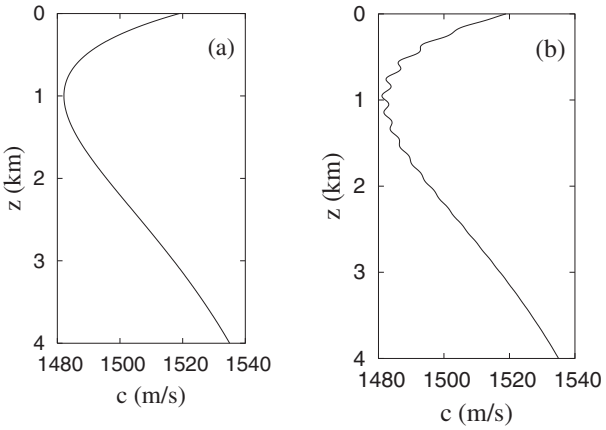

FIG. 1. Sound-speed profiles: (a) the unperturbed case and (b) at $r = 1.25$ km with $\varepsilon = 0.005$.

$$\frac{dp}{dr} = -\frac{\partial H}{\partial z} = -\frac{1}{c_0}\frac{d\Delta c}{dz} - \frac{1}{c_0}\frac{d\delta c}{dz}. \tag{8}$$

The last term in the right-hand side of Eq. (8) can be rewritten in the following form:

$$\frac{1}{c_0}\frac{d\delta c}{dz} = \frac{\varepsilon e^{-2z/B}}{2B}\left[\left(1 - \frac{2z}{B}\right)(\cos\Phi^- - \cos\Phi^+) - k_z z(\sin\Phi^- - \sin\Phi^+)\right], \tag{9}$$

where we denoted $\Phi^\pm = k_z z \pm k_r r$, $k_z = 2\pi/\lambda_z$, and $k_r = 2\pi/\lambda_r$. The smallness of λ_z implies that the range-dependent term oscillates rapidly along a ray path, except for the resonant regions, where either the condition

$$\frac{d\Phi^+}{dr} = k_z p + k_r \simeq 0 \tag{10}$$

or the condition

$$\frac{d\Phi^-}{dr} = k_z p - k_r \simeq 0 \tag{11}$$

is fulfilled. The theory of such resonances was developed in [19,24–29]. Here we only give a brief description of their properties.

Let us consider one of the resonant conditions, for instance, the former one. First we simplify Eq. (9). Since k_z can be thought of as a large parameter, we leave only those terms in the right-hand side, which are proportional to k_z. In addition, we neglect the nonresonant term $\sim\sin\psi^-$. Thus we obtain

$$\frac{dp}{dr} = -\frac{1}{c_0}\frac{d\Delta c}{dz} - \frac{\varepsilon k_z z e^{-2z/B}}{2B}\sin\psi^+. \tag{12}$$

At the next step we shall describe variations of the perturbation phase ψ^+ along a ray path. Using Eqs. (9) and (10) and omitting superscript "+," one derives the pendulumlike equation

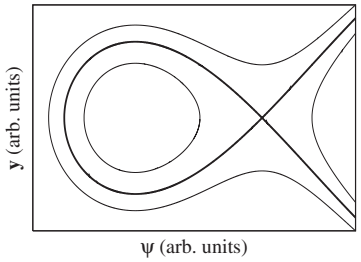

FIG. 2. The phase portrait corresponding to the Hamiltonian (15).

$$\frac{d^2\psi}{dr^2} + \frac{\varepsilon k_z^2 z e^{-2z/B}}{2B}\sin\psi + \frac{k_z}{c_0}\frac{d\Delta c}{dz} = 0. \tag{13}$$

This equation can be rewritten as the coupled pair of first-order equations

$$\frac{d\psi}{dr} = y,$$

$$\frac{dy}{dr} = -\frac{\varepsilon k_z^2 z e^{-2z/B}}{2B}\sin\psi - \frac{k_z}{c_0}\frac{d\Delta c}{dz}, \tag{14}$$

corresponding to the Hamiltonian $\tilde{H}$ of the form

$$\tilde{H}(y,\psi) = \frac{y^2}{2} + \frac{k_z}{c_0}\frac{d\Delta c}{dz}\psi - \frac{\varepsilon k_z^2 z e^{-2z/B}}{2B}\cos\psi, \tag{15}$$

where y and ψ are treated as canonically conjugated momentum and coordinate, respectively. If the inequality

$$\left|\frac{1}{c_0}\frac{d\Delta c}{dz}\right| < \frac{\varepsilon k_z z e^{-2z/B}}{2B} \tag{16}$$

is satisfied, then the phase portrait corresponding to the Hamiltonian (15) contains a resonant area bounded by the separatrix loop (see Fig. 2). A ray can cross the separatrix due to variation of depth z, included in Eqs. (13)–(16) as a slowly-varying parameter. When a ray arrives the resonant area ψ switches its behavior from rotation to oscillation, that is followed by localization of ray momentum in a narrow interval near the resonant value $p_{\text{res}}=-k_r/k_z$. The emphatic point is that each crossing of the resonant area is followed by a jumplike variation of the ray Hamiltonian (6), which depends extremely on the initial conditions; therefore multiple visits to the resonant area cause chaotic ray diffusion in the underlying phase space.

The formulas (10) and (16) allow one to distinguish the rays affected by the resonance. The inequality (16) is fulfilled only near the waveguide axis, where $d\Delta c/dz=0$. The ray momentum at the axis is given by the equation

$$p(z=z_a,H_0) = \sqrt{2E + \frac{b^2(\mu-\gamma)^2}{4}}, \tag{17}$$

where z_a is the depth of the channel axis (5), and the parameter

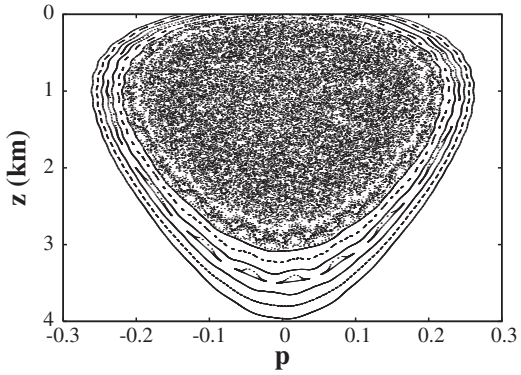

FIG. 3. Poincaré map with $\varepsilon=0.005$.

$$E = 1 + H \simeq 1 + H|_{\delta c=0} \tag{18}$$

can be referred to as the "energy" of ray oscillations in a waveguide. Substituting Eq. (17) into Eq. (10), we find the resonant value of E,

$$E_{\text{res}} = \frac{\lambda_z^2}{2\lambda_r^2} - \frac{b^2(\mu-\gamma)^2}{8}. \tag{19}$$

Note that formula (19) relates to the resonance (11) as well. The conditions (10) and (11) differ by the sign of resonant momentum, the former arises at $p<0$, while the latter takes place at $p>0$. It means that these resonances affect the same rays, but they act at different phases of a trajectory. With $\lambda_z=0.2$ km and $\lambda_r=5$ km the condition (19) holds for near-axial rays. According to Fig. 3, resonances (10) and (11) cause a wide chaotic sea in phase space, without considerable stable islands within. Therefore one can assume that chaotic diffusion of rays inside the sea is close to ergodic mixing.

IV. FLOQUET MODES

Mixing ray dynamics anticipates fast decoherence and spreading of a wave packet initially located within the chaotic sea, until all the area of the sea will be covered [20]. Certainly, it is the case in the short wavelength limit, when ray and wave descriptions are well correlated [21,30]. The question we ask is how the chaotic sea reveals itself at relatively low frequencies, when influence of diffraction and interference is non-negligible, and one-to-one correspondence between a wave pattern and its semiclassical approximation should not be expected. To address this issue, we shall analyze phase space structure of the Floquet modes, which were first applied for studying underwater sound propagation in [15,31]. The Floquet modes can be cast in the form

$$u_m(z,r) = e^{i\alpha_m r/\lambda_r}\Psi_m(z,r), \tag{20}$$

where $m=1,2,\ldots$, $\Psi_m(z,r)=\Psi_m(z,r+\lambda_r)$, and α_m is a real constant. The Floquet modes u_m are the eigenfunctions of the shift operator $\hat{F}$, defined as

$$\hat{F}\phi(z,r) = \phi(z,r+\lambda_r). \tag{21}$$

In the present paper we consider the functions

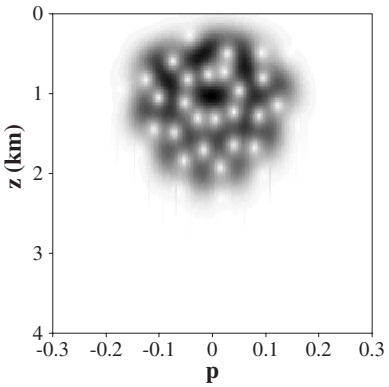

FIG. 4. Floquet mode with the largest number of principal components, $\varepsilon=0.005$.

$$\Phi_m(z) = \Psi_m(z, r=0). \tag{22}$$

Each of these functions can be expanded in some orthogonal basis,

$$\Phi_m(z) = \sum_l c_{lm}\phi_l(z), \tag{23}$$

where $c_{1m}, c_{2m}, \ldots$ are the components of the mth eigenvector of the matrix with elements

$$F_{mn} = \int_{z=0}^{h} \phi_m(z)\hat{F}\phi_n(z)dz. \tag{24}$$

Here $\hat{F}\phi_n(z)$ is the solution of the parabolic equation at the range $r=\lambda_r$ with initial condition $\phi(z, r=0)=\phi_n(z)$. We found the set of functions ϕ_n by solving the Sturm-Liouville problem

$$\frac{\partial^2\phi_n}{\partial z^2} + 2k_0^2\left(E_n - \frac{\Delta c}{c_0}\right)\phi_n = 0. \tag{25}$$

The solution is the following:

$$\phi_n(\xi) = A_n e^{-\xi/2}\xi^{s_n} G(1-n,\ 2s_n+1,\ \xi), \tag{26}$$

where n is a positive integer, ξ is linked with depth by formula

$$\xi(z) = \frac{2k_0}{b}ae^{-az}, \tag{27}$$

A_n is the normalization constant, determined by the condition

$$\int \phi_n\phi_n^* dz = 1, \tag{28}$$

$G(1-n,\ 2s_n+1,\ \xi)$ is the degenerate hypergeometric function, and the parameter s_n is given by the expression

$$s_n = \frac{k_0}{a}\sqrt{\frac{\mu\gamma b^2}{2} - E_n}. \tag{29}$$

Eigenvalues of the parameter E are given by the following expression:

$$E_n = \frac{\mu\gamma b^2}{2} - \frac{1}{2}\left[b\frac{\mu+\gamma}{2} - \frac{a}{k_0}\left(n+\frac{1}{2}\right)\right]^2. \tag{30}$$

At small n the functions ϕ_n coincide with normal modes of the unperturbed waveguide.

Phase space representation of the Floquet modes can be obtained by use of the Husimi distribution function

$$W_h(z,p,r) = \left|\frac{1}{\sqrt[4]{2\pi\Delta_z^2}}\int dz'\,\phi_n(z',r) \times \exp\left(ik_0p(z'-z) - \frac{(z'-z)^2}{4\Delta_z^2}\right)\right|^2. \tag{31}$$

Here Δ_z is the smoothing scale, which we took as 100 m.

Before analyzing the Floquet modes, it is necessary to define a criterion by which we shall determine their chaoticity. The simplest way is to compare phase space location of a Floquet mode with classical phase space structures [32]. We shall use the criterion of Leboeuf and Voros [33–35], identifying the chaotic Floquet state by irregular distribution of zeroes of the Husimi function. Husimi zeroes of regular Floquet states are located along curves. For the sake of a convenient representation, we shall analyze the distribution of Husimi zeroes in the space of the action and angle variables. The action and angle variables are introduced by the following formulas:

$$I = \frac{1}{2\pi}\oint pdz, \quad \theta = \frac{\partial}{\partial I}\int_{z_0}^{z} pdz. \tag{32}$$

The action variable I measures steepness of a ray trajectory and is equal to 0 for the horizontal axial ray. In the integrable limit all the Husimi zeroes are distributed along horizontal lines $I=$const. We shall restrict ourselves by only qualitative analysis of the Husimi zeroes in the range of small values of the action, where the chaotic sea takes place. The exact analytical expressions for the action and angle variables are presented in the Appendix.

In addition, we shall calculate the so-called number of principal components [36]. For the Floquet mode with number m, it is determined by the formula

$$\Gamma(m) = \frac{1}{\sum_l |c_{lm}|^4}. \tag{33}$$

This quantity measures delocalization of a Floquet mode with respect to the basis of the eigenfunctions (26), and also may be treated as a measure of chaoticity. Roughly speaking, Γ is the number of eigenmodes of the unperturbed waveguide, which give the dominant contribution into a given Floquet mode. Chaotic Floquet modes, being formed by a large number of waveguide eigenmodes, are characterized by large values of Γ [15].

Let us start with considering the frequency of 100 Hz. Despite of strong chaos in the ray limit, the majority of the Floquet modes are localized within narrow bands in phase space with Γ ranging from 1 to 2. Only few Floquet modes spread over the chaotic layer. The most extended Floquet mode, having the largest number of principal components

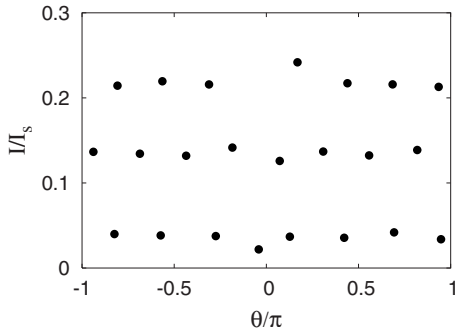

FIG. 5. Distribution of Husimi zeroes for the Floquet mode depicted in Fig. 4 in the plane of normalized initial values of the action and angle. I_s is the most accessible value of the action for guided rays.

$(\Gamma \simeq 4)$, is presented in Fig. 4. Its Husimi zeroes, though covering a wide area, are located along almost horizontal curves; this is shown in Fig. 5. Therefore we can regard this mode rather as weakly irregular than chaotic.

Regular Floquet modes were found in all the phase space regions corresponding to guided rays, even inside the chaotic sea. Let us pay attention to those Floquet modes, which have a "dial-plate" structure, as is shown in Fig. 6. This structure consists of eight well-resolved and ordered peaks. The angular locations of the peaks in Figs. 6(a) and 6(b) are different; the peaks in the upper plot correspond to the zeroes in the lower one, and vice versa.

The origin of the peaks can be clarified if we construct the Poincaré map with a decreased amplitude of the range-dependent perturbation $\varepsilon=0.0005$. This map is presented in Fig. 7. A bare comparison of Figs. 6 and 7 yields that peaks in Fig. 6(a) are allocated near the elliptic fixed points of the resonance 1:8, while peaks in Fig. 6(b) are placed near the hyperbolic ones. As it follows from Fig. 3, this resonance is completely destroyed with $\varepsilon=0.005$. Another argument for the link between "dial-plate" structure and resonance 1:8 is presented in Fig. 8. There it is shown that eight Husimi zeroes of the mode, presented in Fig. 6(a), lay on the horizontal line $I=I_{\mathrm{res}}$, where I_{res} is the resonant action, satisfying the equation

$$m\omega(I=I_{\mathrm{res}})=nk_r, \tag{34}$$

with $m=8$ and $n=1$. Here ω is the spatial frequency of ray oscillations in the waveguide. For the resonance 1:8 we have

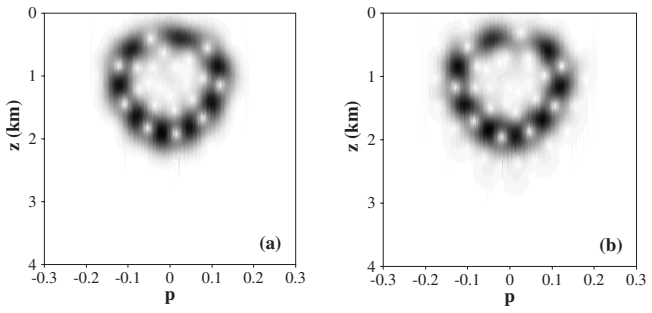

FIG. 6. Floquet modes with "dial-plate" structure. The signal frequency is of 100 Hz, $\varepsilon=0.005$.

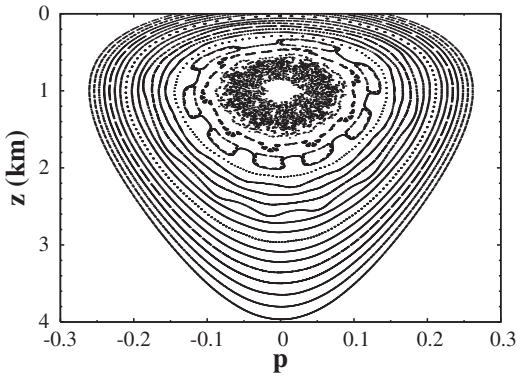

FIG. 7. Poincaré map with $\varepsilon=0.0005$.

$I_{\mathrm{res}} \simeq 0.2I_s$, where I_s is the most accessible action for rays propagating without reflections from the lossy bottom. Hence one may conclude that the peaks in the Husimi plots relate to the so-called scarred states [37,38].

However, this interpretation is problematic, because increasing of ε drastically alters the phase space distribution of periodic orbits. We demonstrate it by constructing the map representing variations of ray action per ray cycle length as a function of initial coordinates in phase space [12,13]. These maps can be used for detecting periodic orbits. The respective plots with $\varepsilon=0.0005$ and 0.005 are presented in Figs. 9 and 10. All the periodic orbits belong to the zero lines separating the regions of negative and positive variations of action. Approximate locations of elliptic and hyperbolic periodic orbits may be found as intersections of the zero lines with horizontal lines $I/I_s=I_{\mathrm{res}}/I_s$. Figures 9(b) and 10(b) represent variations of the action along that line.

As it follows from Fig. 9, the map is smooth with $\varepsilon=0.0005$, and intersections with the horizontal bold line 1:8 are well-ordered. In contrast, the map with $\varepsilon=0.005$ (see Fig. 10) displays a very complicated "wavelike" pattern, and intersections with the bold line have dense and irregular distribution. Obviously, these intersections cannot be associated with elliptic and hyperbolic fixed points of KAM resonance 1:8. As a consequence, periodic orbits are disordered. This is demonstrated in Fig. 11, where we show phase space locations of periodic orbits in the range of low values of the action. Evidently, the bright spots in the Husimi plots for the Floquet modes do not correspond to certain periodic orbits.

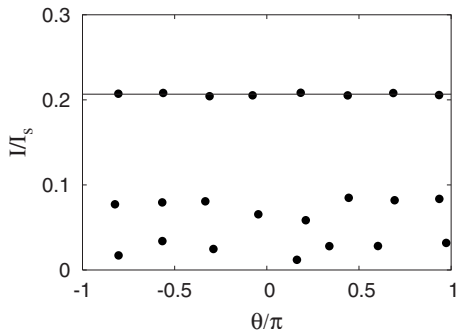

FIG. 8. Distribution of Husimi zeroes for the Floquet mode depicted in Fig. 6(a). The horizontal line corresponds to the resonance 1:8.

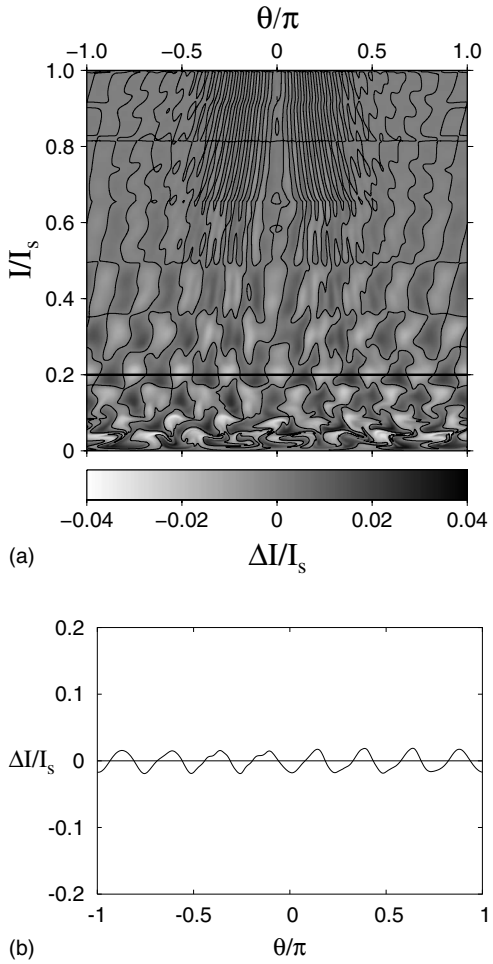

FIG. 9. (a) Variations of the normalized action $\Delta I/I_s$ per ray cycle length in the plane of normalized initial values of the action and angle with $\varepsilon=0.0005$. The horizontal bold line corresponds to KAM resonance 1:8. Thin lines mark zero variations of the action. (b) Variations of the normalized action along the bold line.

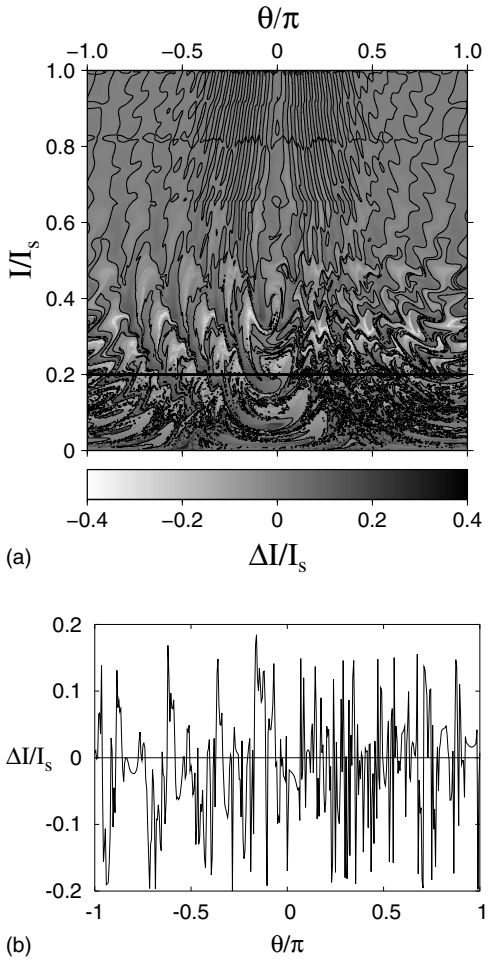

FIG. 10. The same as in Fig. 9, but with $\varepsilon=0.005$.

Floquet modes having the same "dial-plate" structure were also found with the frequencies of 70 and 50 Hz (see Figs. 12 and 13). In these cases the Floquet modes do not possess any hallmarks of chaos.

Our explanation of the well-ordered peaks in the Husimi plots is the following. Decreasing of the signal frequency makes wave refraction less sensitive to small-scale vertical oscillations of the sound-speed perturbation. As it was shown in the previous section, these oscillations are responsible for strong chaos of near-axial rays. Hence the main source of chaos is suppressed at low frequencies. Enhancing of ray-wave correspondence requires smoothing of fast vertical oscillations using some averaging technique. Evidently, the averaging of fast oscillations means replacement of the original sound-speed perturbation by the smoothed one with a lower amplitude. This implies that the disordered multiplication of periodic orbits should be removed, and the well-ordered periodic orbits of completely destroyed resonance 1:8 should be restored. Thus the decreasing of frequency leads to the similar effect as the decreasing of the perturbation's amplitude and is followed by recovery of periodic orbits and occurrence of the peaks observed. In some sense, peaks of the Floquet modes may be regarded as some specific kind of scars.

V. CONCLUSION

In the present paper we have considered sound wave motion in an acoustic waveguide with the range-dependent sound-speed perturbation imposed. It is shown that small-scale vertical oscillations of the perturbation influence near-axial rays in a resonant way. Scattering on resonance makes

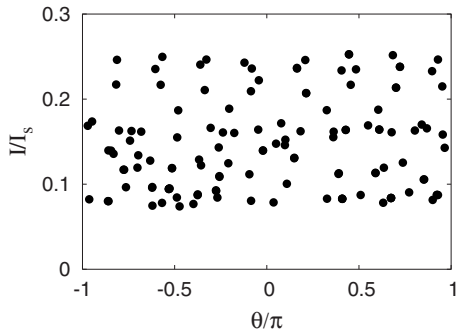

FIG. 11. Phase space locations of periodic orbits, computed with $\varepsilon=0.005$.

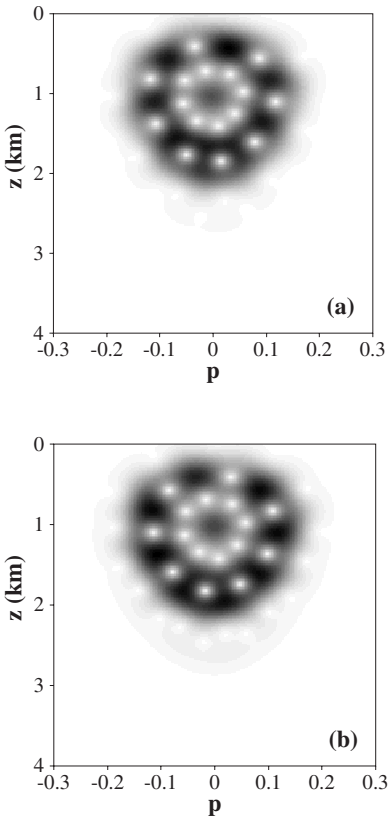

FIG. 12. Floquet modes with "dial-plate" structure. The signal frequency is of 70 Hz, $\varepsilon=0.005$.

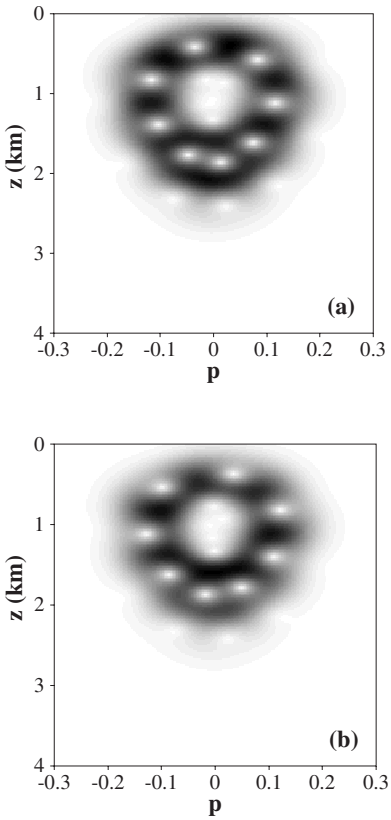

FIG. 13. Floquet modes with "dial-plate" structure. The signal frequency is of 50 Hz, $\varepsilon=0.005$.

near-axial rays unstable and leads to the forming of a wide chaotic sea in the underlying phase space, without any considerable islands of stability. Moreover, small-scale vertical oscillations of the perturbation cause proliferation and disordered phase space distribution of periodic orbits. Nevertheless, the majority of the Floquet modes calculated with frequencies of 50–100 Hz reveals a regular pattern with ordered peaks and Husimi zeroes. The peaks are located near the elliptic or hyperbolic fixed points of the "classical" KAM 1:8. This is confirmed by constructing the Poincaré map with lower amplitude of the perturbation. However, the peaks observed are not associated with certain periodic orbits in the original case. That resonance, as well as its periodic orbits, is completely destroyed with a nondecreased amplitude of the sound-speed perturbation. Thus we are faced with an eccentric conflict of ray and wave descriptions: the peaks have specific "classical" resonant topology but are not supported by classical periodic orbits.

In our opinion, the revival of KAM resonance 1:8 on the Husimi plots indicates the necessity of frequency-dependent corrections to the standard ray approximation, when ray motion is strongly affected by small-scale features. A likely way of introducing such corrections is the construction of some effective sound-speed profile, using the homogenization procedures [39], or exploiting the quantum action [40]. We suppose that ray modeling with the effective sound-speed profile should be more consistent with wave pattern. In particular, a corrected ray approximation may provide the desirable link between the Husimi peaks and the respective periodic orbits. Our expectations are partially supported by the numerical simulation, presented in [23], where it was shown that smoothing of fine-scale structures does not lead to significant changes in a wave field. As a concluding remark, it should be mentioned that the stabilizing of wave refraction with decreasing frequency seems to be worth overcoming limitations on the hydroacoustical tomography, which are posed by ray chaos [41].

ACKNOWLEDGMENTS

This work was supported by the projects of the President of the Russian Federation, by the Program "Mathematical Methods in Nonlinear Dynamics" of the Prezidium of the Russian Academy of Sciences, and by the Program for Basic Research of the Far Eastern Division of the Russian Academy of Sciences. The authors are grateful to S.V. Prants, A.I. Neishtadt, A.L. Virovlyansky, and A.I. Gudimenko for helpful discussions during the course of this research.

APPENDIX

The action and angle variables for the rays propagating without reflections from the ocean surface are given by the formulas

$$I=\frac{b}{a}\left(\frac{\mu+\gamma}{2}-\sqrt{\mu\gamma-\frac{2E}{b^2}}\right), \tag{A1}$$

$$\theta = \pm \frac{\pi}{2} \mp \theta_1, \tag{A2}$$

where the quantities Q and θ_1 are given by the formulas

$$Q = \sqrt{(\mu - \gamma)^2 + \frac{8E}{b^2}}, \tag{A3}$$

$$\theta_1 = \arcsin\left(\frac{\mu + \gamma - (2\mu\gamma - 4E/b^2)e^{az}}{Q} \right). \tag{A4}$$

The upper and lower signs in Eq. (A2) correspond to positive and negative values of ray momentum, respectively. The action and the angle for surface-bounce rays are given by the following formulas:

$$I = \frac{b}{a}\left(\frac{\mu + \gamma}{4} - \frac{\mu + \gamma}{2\pi}\arcsin\frac{\mu + \gamma - 2}{Q} - \frac{\pi + 2\theta_2}{2\pi}\sqrt{\mu\gamma - \frac{2E}{b^2}} \right) + \frac{|p(z=0)|}{\pi a}, \tag{A5}$$

$$\theta = \pm \pi \frac{\theta_2 - \theta_1}{\theta_2 + \pi/2}. \tag{A6}$$

In Eqs. (A5) and (A6) we used the notation

$$\theta_2 = \arcsin\left(\frac{\mu + \gamma - 2\mu\gamma + 4E/b^2}{Q} \right). \tag{A7}$$

Under reflections, ray momentum is given by the formula

$$p(z=0) = \pm \sqrt{2E - b^2(\mu - 1)(\gamma - 1)}. \tag{A8}$$

The inverse transformation for the rays, propagating without reflections from the surface, is expressed as follows:

$$z(I, \theta) = \frac{1}{a}\ln\frac{a^2 b^2(\mu + \gamma - Q\cos\theta)}{2\omega^2}, \tag{A9}$$

$$p(I, \theta) = \frac{\omega Q \sin\theta}{a(\mu + \gamma - Q\cos\theta)}, \tag{A10}$$

where ω is the spatial frequency of ray oscillations in a waveguide. It depends on E in the following way:

$$\omega = ab\sqrt{\mu\gamma - 2E/b^2}. \tag{A11}$$

[1] P. B. Wilkinson, T. M. Fromhold, R. P. Taylor, and A. P. Micolich, Phys. Rev. E **64**, 026203 (2001).
[2] L. Klimes, Pure Appl. Geophys. **159**, 1465 (2002).
[3] M. Bottigliery, S. De Martino, M. Falanga, and C. Godano, Nonlinear Processes Geophys. **12**, 1003 (2005).
[4] S. S. Abdullaev and G. M. Zaslavsky, Sov. Phys. Usp. **34**, 645 (1991).
[5] H. J. Stöckman, *Quantum Chaos: An Introduction* (Cambridge University Press, Cambridge, England, 1999).
[6] A. V. Chigarev and Yu. V. Chigarev, Sov. Phys. Acoust. **24**, 432 (1978).
[7] D. R. Palmer, M. G. Brown, F. D. Tappert, and H. F. Bezdek, Geophys. Res. Lett. **15**, 569 (1988).
[8] M. G. Brown, J. A. Colosi, S. Tomsovic, A. L. Virovlyansky, M. A. Wolfson, and G. M. Zaslavsky, J. Acoust. Soc. Am. **113**, 2533 (2003).
[9] F. J. Beron-Vera, M. G. Brown, J. A. Colosi, S. Tomsovic, A. L. Virovlyansky, M. A. Wolfson, and G. M. Zaslavsky, J. Acoust. Soc. Am. **114**, 1226 (2003).
[10] I. P. Smirnov, A. L. Virovlyansky, and G. M. Zaslavsky, Phys. Rev. E **64**, 036221 (2001).
[11] D. V. Makarov, M. Yu. Uleysky, M. V. Budyansky, and S. V. Prants, Phys. Rev. E **73**, 066210 (2006).
[12] D. V. Makarov and M. Yu. Uleysky, J. Phys. A **39**, 489 (2006).
[13] D. V. Makarov, M. Yu. Uleysky, and S. V. Prants, Chaos **14**, 79 (2004).
[14] A. L. Virovlyansky and G. M. Zaslavsky, Phys. Rev. E **59**, 1656 (1999).
[15] I. P. Smirnov, A. L. Virovlyansky, M. Edelman, and G. M. Zaslavsky, Phys. Rev. E **72**, 026206 (2005).
[16] A. L. Virovlyansky, J. Acoust. Soc. Am. **113**, 2523 (2003).
[17] F. J. Beron-Vera and M. G. Brown, J. Acoust. Soc. Am. **115**, 1068 (2004).
[18] R. A. Vadov, Acoust. Phys. **46**, 544 (2000).
[19] D. V. Makarov and M. Yu. Uleysky, Acoust. Phys. **53**, 495 (2007).
[20] M. Latka, P. Grigolini, and B. J. West, Phys. Rev. A **47**, 4649 (1993).
[21] B. Sundaram and G. M. Zaslavsky, Chaos **9**, 483 (1999).
[22] A. Bäcker, R. Ketzmerick, and A. G. Monastra, Phys. Rev. Lett. **94**, 054102 (2005).
[23] K. C. Hegewisch, N. R. Cerruti, and S. Tomsovic, J. Acoust. Soc. Am. **117**, 1582 (2005).
[24] A. P. Itin, A. I. Neishtadt, and A. A. Vasiliev, Physica D **141**, 281 (2000).
[25] A. I. Neishtadt, Proc. Steklov Inst. Math. **250**, 183 (2005).
[26] D. V. Makarov and M. Yu. Uleysky, JETP Lett. **83**, 522 (2006).
[27] D. L. Vainchtein, A. I. Neishtadt, and I. Mezic, Chaos **16**, 043123 (2006).
[28] D. V. Makarov and M. Yu. Uleysky, Phys. Rev. E **75**, 065201(R) (2007).
[29] D. V. Makarov and M. Yu. Uleysky, in *Nonlinear Science and Complexity*, edited by A. C. Luo, L. Dai, and H. R. Hamidzadeh (World Scientific, Singapore, 2007); Commun. Nonlinear Sci. Numer. Simul. **13**, 400 (2008).
[30] S. V. Prants and M. Yu. Uleysky, JETP Lett. **82**, 748 (2005).
[31] I. P. Smirnov, A. L. Virovlyansky, and G. M. Zaslavsky, Chaos **14**, 317 (2004).
[32] R. Ketzmerick, L. Hufnagel, F. Steinbach, and M. Weiss, Phys. Rev. Lett. **85**, 1214 (2000).
[33] P. Leboeuf and A. Voros, J. Phys. A **23**, 1765 (1990).

[34] F. J. Arranz, F. Borondo, and R. M. Benito, Phys. Rev. E **54**, 2458 (1996).
[35] D. Biswas and S. Sinha, Phys. Rev. E **60**, 408 (1999).
[36] A. Sugita and H. Aiba, Phys. Rev. E **65**, 036205 (2002).
[37] E. J. Heller, Phys. Rev. Lett. **53**, 1515 (1984).
[38] E. B. Bogomolny, Physica D **31**, 169 (1988).
[39] G. Allaire and M. Vanninathan, e-print arXiv:math-ph/0510083.
[40] L. A. Caron, D. Huard, G. Melkonyan, K. J. Moriarty, and L. P. Nadeau, J. Phys. A **37**, 6251 (2004).
[41] F. D. Tappert and Xin Tang, J. Acoust. Soc. Am. **99**, 185 (1996).